Scalable Exact Inference in Multi-Output Gaussian Processes

Wessel P. Bruinsma [1 2]   **Eric Perim** [2]   **Will Tebbutt** [1]   **J. Scott Hosking** [3 4]   **Arno Solin** [5]   **Richard E. Turner** [1 6]

Abstract

Multi-output Gaussian processes (MOGPs) leverage the flexibility and interpretability of GPs while capturing structure across outputs, which is desirable, for example, in spatio-temporal modelling. The key problem with MOGPs is their computational scaling $O(n^3 p^3)$, which is cubic in the number of both inputs n (*e.g.*, time points or locations) and outputs p. For this reason, a popular class of MOGPs assumes that the data live around a low-dimensional linear subspace, reducing the complexity to $O(n^3 m^3)$. However, this cost is still cubic in the dimensionality of the subspace m, which is still prohibitively expensive for many applications. We propose the use of a sufficient statistic of the data to accelerate inference and learning in MOGPs with orthogonal bases. The method achieves *linear* scaling in m in practice, allowing these models to scale to large m without sacrificing significant expressivity or requiring approximation. This advance opens up a wide range of real-world tasks and can be combined with existing GP approximations in a plug-and-play way. We demonstrate the efficacy of the method on various synthetic and real-world data sets.

1. Introduction

Gaussian processes (GPs, Rasmussen & Williams, 2006) form an interpretable, modular, and tractable probabilistic framework for modelling nonlinear functions. They are successfully applied in a wide variety of single-output problems: they can automatically discover structure in signals (Duvenaud, 2014), achieve state-of-the-art performance in regression tasks (Bui et al., 2016), enable data-efficient models in reinforcement learning (Deisenroth & Rasmussen, 2011), and support many applications in probabilistic numerics

(Hennig et al., 2015), such as in optimisation (Brochu et al., 2010) and quadrature (Minka, 2000).

Multi-output Gaussian processes (MOGPs) leverage the flexibility and interpretability of GPs while capturing structure across outputs. One of the first applications of GPs with multiple outputs was in geostatistics (Matheron, 1969). Today, MOGPs models can be found in various areas, including geostatistics (Wackernagel, 2003), factor analysis (Teh & Seeger, 2005; Yu et al., 2009), dependent or multitask learning (Boyle & Frean, 2005; Bonilla et al., 2007; 2008; Osborne et al., 2008), latent force models (Álvarez et al., 2009; Álvarez & Lawrence, 2009; Álvarez et al., 2010; Álvarez & Lawrence, 2011), state space modelling (Särkkä et al., 2013), regression networks (Wilson et al., 2012; Nguyen & Bonilla, 2014; Dezfouli et al., 2017), and mixture models (Ulrich et al., 2015; Bruinsma, 2016; Parra & Tobar, 2017; Requeima et al., 2019).

A key practical problem with existing MOGPs is their computational complexity. For n input points, each having p outputs, inference and learning in general MOGPs take $O(n^3 p^3)$ time and $O(n^2 p^2)$ memory, although these may be alleviated by a wide range of approximations (Candela & Rasmussen, 2005; Titsias, 2009; Lázaro-Gredilla et al., 2010; Hensman et al., 2013; Wilson & Nickisch, 2015; Bui et al., 2017; Cheng & Boots, 2017; Hensman et al., 2018). To mitigate these unfavourable scalings, a particular class of MOGPs, which we call the Instantaneous Linear Mixing Model (ILMM, Sec. 2.1), assumes that the data live around an m-dimensional linear subspace, where $m < p$. This class exploits the low-rank structure of its covariance to reduce the complexity of inference and learning to roughly $O(n^3 m^3)$ time and $O(n^2 m^2)$ memory. Although m is typically much smaller than p, the runtime complexity is again cubic in m. Consequently, the ILMM is prohibitively expensive in applications where moderate m is required. Consider, for example, hourly real-time electricity prices at 2313 different locations across 15 U.S. states and the Canadian province of Manitoba during the year 2019 (MISO, 2019). Forecasting electricity prices is crucial in the planning of energy transmission, which happens 24 hours in advance. The ILMM is particularly well suited to this task: the prices derive from optimal power flow, which tends to exhibit low-rank structure. However, it still takes roughly $m = 40$ to explain 95% of the variance of this data. For $n = 1\,\mathrm{k}$ time points, this

---

[1]University of Cambridge [2]Invenia Labs [3]British Antarctic Survey [4]Alan Turing Institute [5]Aalto University [6]Microsoft Research. Correspondence to: Wessel P. Bruinsma <wpb23@cam.ac.uk>.

requires the inversion of a $40\,\mathrm{k} \times 40\,\mathrm{k}$ matrix. Even worse, to explain 99% of the variance, it requires the inversion of a $120\,\mathrm{k} \times 120\,\mathrm{k}$ matrix, clearly far beyond what is feasible.

In this paper, we develop a new perspective on MOGPs in the Instantaneous Linear Mixing Model class through the use of a sufficient statistic of the data. We use this sufficient statistic to identify a class of MOGPs, which we call the Orthogonal Instantaneous Linear Mixing Model (OILMM, Sec. 3), in which inference and learning take $O(n^3m + nmp + m^2p)$ time and $O(n^2m + np + mp)$ memory, without sacrificing significant expressivity nor requiring any approximations. The dominant (first) terms in these expressions are *linear* in m, rather than cubic. It is this feature that allows the OILMM to scale to large m. The linear scaling is achieved by breaking down the high-dimensional multi-output problem into independent single-output problems, whilst retaining exact inference. Consequently, the proposed methodology is interpretable—*e.g.*, it can be seen as a natural generalisation of probabilistic principal component analysis (PPCA, Tipping & Bishop, 1999)—simple to implement, and trivially compatible with single-output scaling techniques in a plug-and-play way. For example, it can be combined with the variational inducing point approximation by (Titsias, 2009) or with state-space approximation methods (Sec. 3.9); these approximations reduce the time complexity of the dominant term to linear in *both* the number of data points n and m. We demonstrate the efficacy of the OILMM in experiments on various synthetic and real-world data sets. Simple algorithms to perform inference and learning in the OILMM are presented in App. A.

2. Multi-Output Gaussian Process Models

For tasks with p outputs, multi-output Gaussian processes induce a prior distribution over *vector-valued* functions $f : \mathcal{T} \to \mathbb{R}^p$ by requiring that any finite collection of function values $f_{p_1}(t_1), \ldots, f_{p_n}(t_n)$ with $(p_i)_{i=1}^n \subseteq \{1, \ldots, p\}$ are multivariate Gaussian distributed. We consider the input space time, where $\mathcal{T} = \mathbb{R}$, but the analysis trivially applies to more general feature spaces, *e.g.* $\mathcal{T} = \mathbb{R}^d$. A MOGP $f \sim \mathcal{GP}(m, K)$ is described by a *vector-valued* mean function $m(t) = \mathbb{E}[f(t)]$ and a *matrix-valued* covariance function $K(t, t') = \mathbb{E}[f(t)f^\mathsf{T}(t')] - \mathbb{E}[f(t)]\mathbb{E}[f^\mathsf{T}(t')]$. For n observations $y(t_1), \ldots, y(t_n) \in \mathbb{R}^p$, inference and learning take $O(n^3p^3)$ time and $O(n^2p^2)$ memory.

2.1. The Instantaneous Linear Mixing Model

A simple, but general class of MOGPs decomposes a signal $f(t)$ comprising p outputs into a fixed basis $h_1, \ldots, h_m \in \mathbb{R}^p$ with coefficients $x_1(t), \ldots, x_m(t) \in \mathbb{R}$:

$$f(t) = h_1 x_1(t) + \ldots + h_m x_m(t) = Hx(t)$$

where h_i is the ith column of H. The coefficients $x_1(t), \ldots,$ $x_m(t)$ are time varying and modelled independently with unit-variance Gaussian processes. The noisy signal $y(t)$ is then generated by adding $\mathcal{N}(0, \Sigma)$-distributed noise to $f(t)$. Intuitively, this means that the p-dimensional data live in a "pancake" (Roweis & Ghahramani, 1999; MacKay, 2002) around the m-dimensional column space of H, where typically $m \ll p$.

Mod. 1 (Instantaneous Linear Mixing Model). Let K be an $m \times m$ diagonal multi-output kernel with $K(t, t) = I_m$, H a $p \times m$ matrix, and Σ a $p \times p$ observation noise covariance. Then the ILMM is given by the following generative model:

$$x \sim \mathcal{GP}(0, K(t, t')), \qquad \text{(latent processes)}$$
$$f(t) \,|\, H, x(t) = Hx(t), \qquad \text{(mixing mechanism)}$$
$$y \,|\, f \sim \mathcal{GP}(f(t), \delta[t - t']\Sigma). \qquad \text{(noise model)}$$

We call x the *latent processes* and H the *mixing matrix* or *basis*. Throughout the paper, we assume that H has linearly independent columns. If we marginalise out f and x, we find that $y \sim \mathcal{GP}(0, HK(t, t')H^\mathsf{T} + \delta[t - t']\Sigma)$, which reveals that the ILMM exhibits low-rank covariance structure. It also shows that the ILMM is a time-varying generalisation of factor analysis (FA): choosing $K(t, t') = \delta[t - t']I_m$ and Σ diagonal recovers FA exactly.

The ILMM is definitely not novel; the specific formulation in Mod. 1 is for convenience of the exposition in this paper. In particular, the ILMM is very similar to the Linear Model of Coregionalisation (LMC) (Goovaerts, 1997). In the LMC, every latent process has multiple independent copies and the observation noise Σ is typically diagonal. More generally, the ILMM is a special case of the more general formulation with mixing mechanism $f(t) = \int \tilde{H}(t, \tau)x(\tau)\,\mathrm{d}\tau$ where $\tilde{H} : \mathcal{T} \times \mathcal{T} \to \mathbb{R}^{p \times m}$ is a matrix-valued time-varying filter. In particular, it is the case $\tilde{H}(t, \tau) = \delta(t - \tau)H$; here the mixing is *instantaneous* and *time-invariant*. Many other MOGPs in the machine learning and geostatistics literature can be seen as specialisations of this more general formulation by imposing structure on $\tilde{H}$ and K. An organisation of the literature from this point of view, which we call the Mixing Model Hierarchy (MMH), is presented in App. B.

2.2. Inference and Learning in the ILMM

The complexities of inference and learning in MOGPs can often be alleviated by exploiting structure in the kernel. This is the case for the ILMM, which we have seen exhibits low-rank covariance structure. In this section, we develop a new perspective on the ILMM by showing that the covariance structure can be exploited by devising a low-dimensional "summary" or "projection" of the p-dimensional observations. This reduces the complexities from $O(n^3p^3)$ time and $O(n^2p^2)$ memory to $O(n^3m^3 + nmp + m^2p)$ time and $O(n^2m^2 + np + mp)$ memory, where $O(nmp + m^2p)$ is

the cost of projecting the data and computing the projection, and $O(np + mp)$ is the cost of storing the data and projection.

The low-dimensional projection of the observations y will be given by a sufficient statistic for the model, which is therefore "without loss of information" and can be used to accelerate inference. Concretely, the projection of y is given by the maximum likelihood estimate (MLE) of x under the likelihood $p(y \mid x)$ of the ILMM. As Prop. 2 in App. D shows, this MLE is given by Ty where T is the $m \times p$ matrix $(H^\mathsf{T}\Sigma^{-1}H)^{-1}H^\mathsf{T}\Sigma^{-1}$; Ty is an unbiased estimator of x. Because Ty is an MLE for x, it is a function of a sufficient statistic for x, if one exists. Prop. 3 in App. E shows that Ty is actually minimally sufficient itself. For any prior $p(x)$ over x, sufficiency of Ty gives that $p(x \mid y) = p(x \mid Ty)$; that is, conditioning on y is equivalent to conditioning on Ty, where Ty can be interpreted as a "summary" or "projection" of y. This idea is formalised in the following proposition, which is proven in App. F:

Prop. 1. Let $p(x)$ be a model for $x \colon \mathcal{T} \to \mathbb{R}^m$, not necessarily Gaussian, H a $p \times m$ matrix, and Σ a $p \times p$ observation noise covariance. Then consider the following generative model:

$$x \sim p(x), \qquad \text{(latent processes)}$$
$$f(t) \mid H, x(t) = Hx(t), \qquad \text{(mixing mechanism)}$$
$$y \mid f \sim \mathcal{GP}(f(t), \delta[t - t']\Sigma). \qquad \text{(noise model)}$$

Consider a $p \times n$ matrix Y of observations of y. Then $p(f \mid Y) = p(f \mid TY)$, where the distribution of the projected observed signal Ty is

$$Ty \mid x \sim \mathcal{GP}(x(t), \delta[t-t']\Sigma_T) \text{ with } \Sigma_T = (H^\mathsf{T}\Sigma^{-1}H)^{-1}.$$

Moreover, the probability of the data Y is given by

$$p(Y) = \left[\prod_{i=1}^n \frac{\mathcal{N}(y_i \mid 0, \Sigma)}{\mathcal{N}(Ty_i \mid 0, \Sigma_T)}\right]\int p(x)\prod_{i=1}^n \mathcal{N}(Ty_i \mid x_i, \Sigma_T)\,\mathrm{d}x$$

where the ith observation y_i is the ith column of Y.

Crucially, Y are p-dimensional observations, TY are m-dimensional summaries, and typically $m \ll p$, so conditioning on TY is often much cheaper; note that computing TY takes $O(nmp)$ time and $O(mp)$ memory. In particular, if we apply Prop. 1 to the ILMM by letting $x \sim \mathcal{GP}(0, K(t, t'))$, we immediately get the claimed reduction in complexities: whereas conditioning on Y takes $O(n^3p^3)$ time and $O(n^2p^2)$ memory, we may equivalently condition on TY, which takes $O(n^3m^3)$ time and $O(n^2m^2)$ memory instead. This important observation is depicted in Fig. 1a.

The case of Prop. 1 where x is Gaussian can be found as Results 1 and 2 by Higdon et al. (2008), and was also used by the authors to accelerate inference. Although the reduction

in computational complexities allows Higdon et al. to scale to significantly larger data, they are still limited by the cubic dependency on m.

If the observations can be naturally represented as multi-index arrays in $\mathbb{R}^{p_1 \times \cdots \times p_q}$, a natural choice is to correspondingly decompose $H = H_1 \otimes \cdots \otimes H_q$ where $\otimes$ is the Kronecker product. In this parametrisation, the projection and projected noise also become the Kronecker products: $T = T_1 \otimes \cdots \otimes T_q$ and $\Sigma_T = \Sigma_{T_1} \otimes \cdots \otimes \Sigma_{T_q}$. See App. H. The model by Zhe et al. (2019) can be seen as an ILMM of this form with $K(t, t') = k(t, t')I_m$ where k is a scalar-valued kernel and $\Sigma = \sigma^2 I_p$.

In Prop. 1, we call $\Sigma_T = T\Sigma T^\mathsf{T} = (H^\mathsf{T}\Sigma^{-1}H)^{-1}$ the *projected observation noise*. The projected noise Σ_T is important, because it couples the latent processes upon observing data. In particular, if the latent processes are independent under the prior and Σ_T is diagonal, then the latent processes remain independent when data is observed. This observation forms the basis of the computational gains achieved by the Orthogonal Instantaneous Linear Mixing Model.

2.3. Interpretation of the Likelihood

Prop. 1 shows that the log-probability of the data Y is equal to the log-probability of the projected data TY plus, for every observation y_i, a correction term of the form $\log \mathcal{N}(y_i \mid 0, \Sigma)/\mathcal{N}(Ty_i \mid 0, \Sigma_T)$. Prop. 4 in App. G shows that this correction term can be written as

$$-\tfrac{1}{2}(p - m)\log 2\pi - \underbrace{\tfrac{1}{2}\log|\Sigma|/|\Sigma_T|}_{\text{noise "lost by projection"}} - \underbrace{\tfrac{1}{2}\|y_i - HTy_i\|_\Sigma^2}_{\text{data "lost by projection"}},$$

where $\|\bullet\|_\Sigma = \|\Sigma^{-\frac{1}{2}}\bullet\|$. When the likelihood is optimised with respect to H, the correction terms will prevent the projection T from discarding a component of the data Y and the noise Σ that is "too large". For example, for the ILMM, if these correction terms were ignored, then after optimising we would find that $TY = 0$ and $\Sigma_T = 0$, because the density of a zero-mean Gaussian is highest at the origin, and becomes higher as the variance becomes smaller; it is exactly $TY = 0$ and $\Sigma_T = 0$ that the two penalties prevent from happening.

3. The Orthogonal Instantaneous Linear Mixing Model

Inspired by Prop. 1, we will now identify a subclass of the ILMM for which, in practice, inference and learning scale *linearly* in the number of latent processes m rather than cubically. As we will see, this happens when the projected observation noise is diagonal, which is the case for the Orthogonal Instantaneous Linear Mixing Model (OILMM): the subclass of ILMMs where the basis H is *orthogonal*. In particular, $H = US^{\frac{1}{2}}$ where U is a matrix with orthonormal
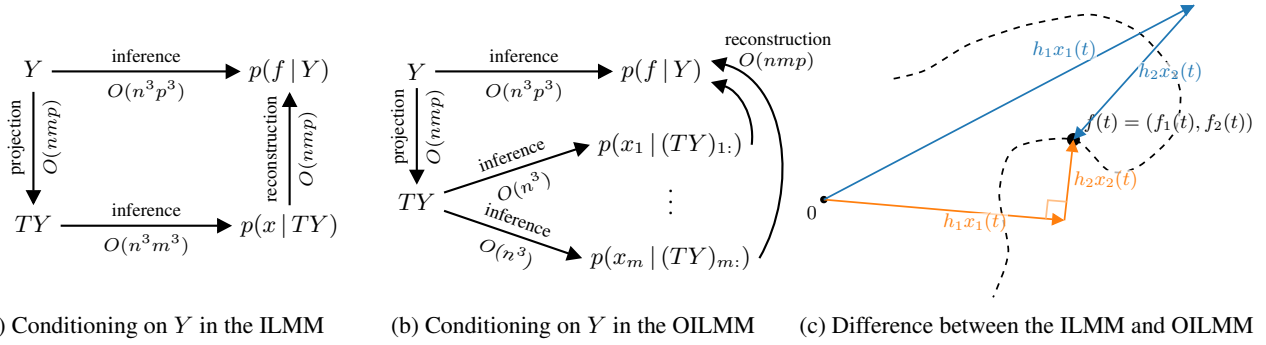
(a) Conditioning on Y in the ILMM   (b) Conditioning on Y in the OILMM   (c) Difference between the ILMM and OILMM

Figure 1. (a–b) Commutative diagrams depicting that conditioning on Y in the ILMM and OILMM is equivalent to conditioning respectively on TY and independently every x_i on $(TY)_{i:}$, but yield different computational complexities. The reconstruction costs assume computation of the marginals. (c) Illustration of the difference between the ILMM and OILMM. The trajectory of a particle (dashed line) in two dimensions is modelled by the ILMM (blue) and OILMM (orange). The noise-free position $f(t)$ is modelled as a linear combination of basis vectors h_1 and h_2 with coefficients $x_1(t)$ and $x_2(t)$ (two independent GPs). In the OILMM, the basis vectors h_1 and h_2 are constrained to be orthogonal; in the ILMM, h_1 and h_2 are unconstrained.

columns and $S > 0$ a diagonal. We define this model as follows:

Mod. 2 (Orthogonal Instantaneous Linear Mixing Model). The OILMM is an ILMM (Mod. 1) where the basis H is a $p \times m$ matrix of the form $H = US^{\frac{1}{2}}$ with U a matrix with orthonormal columns and $S > 0$ diagonal, and $\Sigma = \sigma^2 I_p + HDH^\mathsf{T}$ a $p \times p$ matrix with $D \geq 0$ diagonal.

The difference between the ILMM and the OILMM is illustrated in Fig. 1c. In the OILMM, we require that $m \leq p$, since the number of p-dimensional vectors that can be mutually orthogonal is at most p. Also, D in Σ can be interpreted as heterogeneous noise deriving from the latent processes. Moreover, although H and Σ do not depend on time, our analysis and results trivially carry over to the case where H_t and Σ_t do vary with time. Finally, for the OILMM, Prop. 8 in App. L shows that $T = S^{-\frac{1}{2}}U^\mathsf{T}$ and $\Sigma_T = \sigma^2 S^{-1} + D$.

Whereas the ILMM is a time-varying generalisation of FA, the OILMM can be seen as a time-varying generalisation of probabilistic principal component analysis (PPCA, Tipping & Bishop, 1999): $D = 0$ and $K(t, t') = \delta[t-t']I_m$ recovers the orthogonal solution of PPCA exactly; recall that PPCA admits infinitely many solutions, with only one corresponding to orthogonal axes, whereas the modelling assumptions of the OILMM recover this solution automatically. See Fig. 2 for a visualisation of the relationship between FA, PPCA, the ILMM, and the OILMM. The OILMM is also related to Gaussian Process Factor Analysis (GPFA, Yu et al., 2009), with the crucial difference being that in GPFA orthogonalisation of the columns of H is done as a post-processing step, whereas in the OILMM orthogonality of the columns of H is built into the model. In this respect, the OILMM is more similar to the model by Higdon et al. (2008), who also consider a MOGP with an orthogonal basis built in.
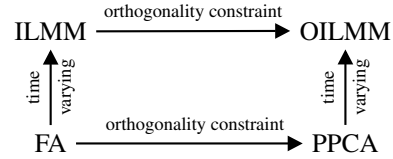

Figure 2. Relationship between factor analysis (FA), probabilistic principal component analysis (PPCA, Tipping & Bishop, 1999), the ILMM (Mod. 1), and the OILMM (Mod. 2)

3.1. Generality of the OILMM

A central theme of the experiments will be to assess how restrictive the orthogonality assumption is for the OILMM. In this section, we theoretically investigate this question from various perspectives. In the separable case, where $K(t, t') = k(t, t')I_m$ for a scalar-valued kernel k, for every ILMM with homogeneous observation noise ($\Sigma = \sigma^2 I_p$), there exists an OILMM with $D = 0$ that is equal in distribution to y. To see this, note

$$y^{(\text{ILMM})} \sim \mathcal{GP}(0, k(t, t')HH^\mathsf{T} + \sigma^2 \delta[t-t']I_p),$$
$$y^{(\text{OILMM})} \sim \mathcal{GP}(0, k(t, t')USU^\mathsf{T} + \sigma^2 \delta[t-t']I_p).$$

Hence, letting USU^T be the eigendecomposition of HH^T gives an OILMM equal in distribution to y. In the non-separable case, where diagonal elements of K are linearly independent, in general only the distribution of $y(t)$ at every t can be recovered by an OILMM, but the correlation between $y(t)$ and $y(t')$ for $t' \neq t$ may be different. In terms of the joint distribution over x and y, which is important for interpretability of the latent processes, Prop. 7 in App. K shows that the Kullback–Leibler (KL) divergence between two ILMMs with bases H and $\hat{H}$ is proportional to $\|H - \hat{H}\|_F^2$, hence symmetric, where $\|\cdot\|_F$ denotes the Frobenius norm. As a consequence (Prop. 7), the KL between an ILMM with basis H and the OILMM closest in

KL is upper bounded by $\|I_m - V\|_F^2$ where V are the right singular vectors of H. This makes sense: $V = I_m$ implies that H is of the form $US^{\frac{1}{2}}$ with U a matrix with orthonormal columns and $S > 0$ diagonal. It also shows that an ILMM is close to an OILMM if V is close to I_m in the sense of the Frobenius norm.

3.2. Choice of Basis

The basis H is a parameter of the model that can be learned through gradient-based optimisation of the likelihood. Parametrising the orthogonal part U of the basis H takes $O(m^2 p)$ time and $O(mp)$ memory (see App. C). This complexity is *quadratic* in m, rather than linear. However, the cost of parametrising U is typically far from dominant, which means that this cost is typically negligible. See App. I for a more detailed discussion.

Observing that $\mathbb{E}[f(t)f^\mathsf{T}(t)] = HH^\mathsf{T}$, a sensible initialisation of the basis H is (a truncation of) $\hat{U}\hat{S}^{\frac{1}{2}}$ where $\hat{\Sigma} = \hat{U}\hat{S}\hat{U}^\mathsf{T}$ is the eigendecomposition of an estimate $\hat{\Sigma}$ of the spatial covariance. In the case that there is a kernel over the outputs, *e.g.* in separable spatio-temporal GP models, H can be set to (a truncation of) $US^{\frac{1}{2}}$ where USU^T is an eigendecomposition of the kernel matrix over the outputs. The hyperparameters of the kernel over the outputs can then be learned with gradient-based optimisation by differentiating through the eigendecomposition. See Sec. 3.9.

3.3. Diagonal Projected Noise

As alluded to in Sec. 2.1, under the OILMM, the projected noise Σ_T from Prop. 1 is diagonal: $\Sigma_T = \sigma^2 S^{-1} + D$; Prop. 6 in the App. J characterises exactly when this is the case. This property is crucial, because, as we explain in the next paragraph, it allows the model to break down the high-dimensional multi-output problem into independent single-output problems, which brings significant computational advantages.

3.4. Inference

Since the projected noise is diagonal, the latent processes remain independent when data is observed. We may hence treat the latent processes independently, conditioning the ith latent process x_i on $(TY)_{i:} = Y^\mathsf{T}U_{i:}/\sqrt{S_{ii}}$ under noise $(\Sigma_T)_{ii} = \sigma^2/S_{ii} + D_{ii}$, which means that the high-dimensional prediction problem breaks down into independent single-output problems. Therefore, inference takes $O(n^3 m + nmp)$ time and $O(n^2 m + np)$ memory (see App. C), which are *linear* in m. This decoupled inference procedure is depicted in Fig. 1b and outlined in more detail in Apps. A.2 and A.3. Note that the decoupled problems can be treated in parallel to achieve sublinear wall time, and that in the separable case further speedups are possible.

3.5. Learning

For computing the marginal likelihood, the OILMM also offers computational benefits. Prop. 9 in App. M shows that $\log p(Y)$ from Prop. 3 simplifies to:

$$\log p(Y)$$
$$= -\frac{n}{2}\log|S| - \frac{n(p-m)}{2}\log 2\pi\sigma^2 - \frac{1}{2\sigma^2}\|(I_p - UU^\mathsf{T})Y\|_F$$
$$+ \sum_{i=1}^m \log \mathcal{N}((TY)_{i:} \mid 0, K_i + (\sigma^2/S_{ii} + D_{ii})I_n)$$

where $\|\cdot\|_F$ denotes the Frobenius norm and K_i is the $n \times n$ kernel matrix for the ith latent process x_i. We conclude that learning also takes $O(n^3 m + nmp)$ time and $O(n^2 m + np)$ memory (see App. C), again *linear* in the number of latent processes. Computation of the marginal likelihood is outlined in more detail in App. A.4.

3.6. Interpretability

Besides computational benefits, the fact that the OILMM breaks down into independent problems for the latent processes also promotes interpretability.[1] Namely, the independent problems can be separately inspected to interpret, diagnose, and improve the model. This is *much* easier than directly working with predictions for the data, which are high dimensional and often strongly correlated between outputs. For example, the OILMM allows a simple and interpretable decomposition of the mean squared error:

$$\underbrace{\|y - Hx\|^2}_{\text{MSE}} = \underbrace{\|P_{H^\perp}y\|^2}_{\substack{\text{data not}\\\text{captured by basis}}} + \sum_{i=1}^m S_{ii}\underbrace{((Ty)_i - x_i)^2}_{\substack{\text{MSE of}\\i^{\text{th}}\text{ latent process}}},$$

where $P_{H^\perp}$ is the orthogonal projection onto the orthogonal complement of $\text{col}(H)$. See Prop. 10 in App. N for a proof.

3.7. Scaling

For both learning and inference, the problem decouples into m independent single-output problems. Therefore, to scale to a large number of data points n, off-the-shelf single-output GP scaling techniques can be trivially applied to these independent problems. For example, if the variational inducing point method by Titsias (2009) is used with $r \ll n$ inducing points, then inference and learning are further reduced to $O(nmr^2)$ time and $O(nmr)$ memory, ignoring the cost of the projection (see App. C). Most importantly, if $k(t, t')$ is Markovian (*e.g.* of the Matérn class), then one can leverage state-space methods to efficiently solve the m independent problems exactly (Hartikainen & Särkkä, 2010; Särkkä & Solin, 2019). This brings down the scaling to $O(nmd^3)$ time and $O(nmd^2)$ memory, where d is the state

---

[1]In the OILMM, the latent processes retain independence in the posterior distribution, which is not generally true for the ILMM.

dimension, typically $d \ll m, n$ (see App. C). We further discuss this approach in Sec. 3.9.

3.8. Missing Data

Missing data is troublesome for the OILMM, because it is not possible to take away a subset of the rows of H and retain orthogonality of the columns. In this section, we develop an approximation for the OILMM to deal with missing data in a simple and effective way. For a matrix or vector A, let A_o and A_m denote the rows of A corresponding to respectively observed and missing values. Also, for a matrix A, let $d[A]$ denote the diagonal matrix resulting from setting the off-diagonal entries of A to zero. In the case of missing data, Prop. 11 in App. O.1 shows that the projection and projected noise are given by $T_o = S^{-\frac{1}{2}} U_o^\dagger$ and $\Sigma_{T_o} = \sigma^2 S^{-\frac{1}{2}} (U_o^\mathsf{T} U_o)^{-1} S^{-\frac{1}{2}} + D$. Observe that Σ_{T_o} is dense, because, unlike U, the columns of U_o are not orthogonal. However, they may be approximately orthogonal, which motivates the approximation $\Sigma_{T_o} \approx d[\Sigma_{T_o}]$. Prop. 12 in App. O.1 shows that this approximation will be accurate if missing observations cannot decrease the norm of a vector in $\mathrm{col}(H)$ too much:

$$\varepsilon_{\mathrm{rel}} = \frac{\|\Sigma_{T_o} - d[\Sigma_{T_o}]\|_{\mathrm{op}}}{\|d[\Sigma_{T_o}]\|_{\mathrm{op}}} \lesssim \max_{y \in \mathrm{col}(H): \|y\|=1} \|y_m\|^2$$

where $\|\cdot\|_{\mathrm{op}}$ denotes the operator norm and $\lesssim$ denotes inequality up to a proportionality constant. For example, if the ith column of H is a unit vector, say e_k, then the bound does not guarantee anything. Indeed, if the kth output is missing, then potentially all information about the ith latent process is lost. On the other hand, if, for example, $\|U\|_\infty^2 \lesssim 1/p$, then Corollary 1 in App. O.1 shows that $\varepsilon_{\mathrm{rel}} \lesssim s/p$ if s outputs are missing, which means that the approximation will be accurate if $s \ll p$. With this approximation, two things change in the log-likelihood (Rem. 1 in App. O.1): for every time point with missing data *(i)* UU^T becomes $U_o U_o^\dagger$ and *(ii)* an extra term $-\frac{1}{2} \log |U_o^\mathsf{T} U_o|$ appears.

It is also easy to use variational inference to handle missing data (App. O.2) and to support heterogeneous observation noise (App. P), but we leave experimental tests of these approaches to future work.

3.9. Application to Separable Spatio–Temporal GPs

Separable spatio–temporal GPs, which are of the form $f \sim \mathcal{GP}(0, k_t(t, t') k_r(r, r'))$, form a vector-valued process $f(t) = (f(t, r_i))_{r=1}^p \sim \mathcal{GP}(0, k_t(t, t') K_r)$ when observed at a fixed number of locations in space, where K_r is the $p \times p$ matrix with $(K_r)_{ij} = k_r(r_i, r_j)$. Letting $U S U^\mathsf{T}$ be the eigendecomposition of K_r, $f(t)$ is an OILMM with $H = U S^{\frac{1}{2}}$ and $K(t, t') = k_t(t, t') I_p$. Note that $m = p$, so the projection takes $O(np^2)$ time (see App. C).
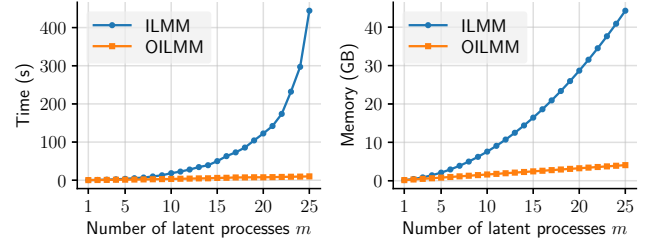

Figure 3. Runtime (left) and memory usage (right) of the ILMM and OILMM for computing the evidence of $n = 1500$ observations for $p = 200$ outputs.

Combining the OILMM framework with efficient state-space scaling techniques (Hartikainen & Särkkä, 2010; Särkkä & Solin, 2019; Solin et al., 2018; Nickisch et al., 2018), which are either exact or arbitrarily good approximations, the complexities are reduced to $O(np^2 + p^3)$ time and $O(np + p^2)$ memory for the entire problem, which are *linear* in n (see App. C). This compares favourably with the filtering techniques of Särkkä et al. (2013) and Hartikainen et al. (2011), both of which have $O(np^3)$ time and $O(np^2)$ memory, and the Kronecker product decomposition (Saatçi, 2012, Ch. 5) approach, which requires $O(p^3 + n^3)$ time and $O(p^2 + n^2)$ memory complexity.

By relaxing K to be a general diagonal multi-output kernel with $K(t, t) = I_p$, we obtain a new class of models which are nonseparable relaxations of the above in which exact inference remains efficient. The orthogonal basis for this OILMM is, as before, the eigenvectors of a kernel matrix whose hyperparameters can be optimised.

4. Experiments

We test the OILMM in experiments on synthetic and real-world data sets. A Python implementation and code to reproduce the experiments is available at `https://github.com/wesselb/oilmm`. A Julia implementation is available at `https://github.com/willtebbutt/OILMMs.jl`.

4.1. Computational Scaling

We demonstrate that exact inference scales favourably in m for the OILMM, whereas the ILMM quickly becomes computationally infeasible as m increases. We use a highly optimised implementation of exact inference for the ILMM, kindly made available by Invenia Labs [2]. Fig. 3 shows the runtime and the memory usage of the ILMM and OILMM. Observe that the ILMM scales $O(m^3)$ in time and $O(m^2)$ in memory, whereas the OILMM scales $O(m)$ in both time and memory. For $m = 25$, the ILMM takes nearly 10 minutes to compute the evidence, whereas the OILMM only requires a couple seconds. See App. Q for more details.
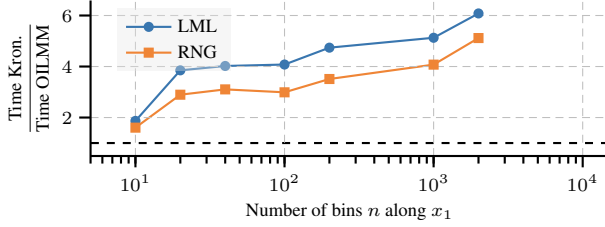
---

[2] `https://invenialabs.co.uk`

Figure 4. Ratio of timings of the Kronecker approach (Saatçi, 2012, Ch. 5) and the OILMM to compute the marginal likelihood of the latent function (LML) and to generate a single prior sample (RNG). See Tab. 5 in App. R for full results.

Table 1. Root-mean-square error (RMSE) and normalised posterior predictive log-probability (PPLP) of held-out test data for the OILMM with varying m and independent GPs (IGP) in the temperature extrapolation experiment. The OILMM achieves parity in RMSE with IGP at $m = 200$ and surpasses it in PPLP at $m = 5$.

	m	1	5	50	100	200	247
RMSE	OILMM	2.151	2.072	2.030	2.002	1.992	1.991
	IGP	1.993	1.993	1.993	1.993	1.993	1.993
PPLP	OILMM	-1.976	-1.457	-0.905	-0.774	-0.600	-0.525
	IGP	-1.923	-1.923	-1.923	-1.923	-1.923	-1.923

4.2. Rainforest Tree Point Process Modelling

We consider a subset of the extensive rain forest data set credited to Hubbell et al. (2005); Condit (1998); Hubbell et al. (1999) in which the locations of 12929 *trichilia tuberculata* have been recorded. This data is modelled via an inhomogeneous Poisson process, whose log-intensity is given a GP prior. Inference is framed in terms of a latent GP with a Poisson likelihood over a discrete collection of bins. The methodology of Solin et al. (2018) is adapted to accelerate inference of the latent processes, which demonstrates the ability of the OILMM to be combined with existing scaling techniques in a plug-and-play fashion. Inference in the kernel parameters and log-intensity process utilise a simple blocked Gibbs sampler.

It takes roughly three hours[3] to perform 10^5 iterations of MCMC (*circa* 10^5 marginal likelihood evaluations and 10^6 prior samples) with 20000 bins, demonstrating the feasibility of a computationally demanding choice of approximate inference procedure. The Kronecker product factorisation technique (Saatçi, 2012, Ch. 5) is a competitive method in this setting, as it can also efficiently and exactly compute log marginal likelihoods and generate prior samples efficiently. Fig. 4 shows the trade off between the two approaches to inference. In this experiment we define $p = n/2$, meaning that the approach described in Sec. 3.9 scales cubically in n. Despite their quite different implementation details, they do obtain similar performance, with the OILMM performing relatively better as n increases. See App. R for further experimental details and analysis.

4.3. Temperature Extrapolation

Having demonstrated that the OILMM offers computational benefits, we now show that the method can scale to large numbers of latent processes ($m = p = 247$) to capture meaningful dependencies between outputs. We consider a simple spatio–temporal temperature prediction problem over Europe. Approximately 30 years worth of the ERA-

Interim reanalysis temperature data[4] (Dee et al., 2011) is smoothed in time with a Hamming window of width 31 and sub-sampled once every 31 days to produce a data set comprising $13 \times 19 = 247$ outputs and approximately 350 months worth of data. We train the OILMM and IGPs (both models use Matérn–$5/2$ kernels with a periodic component) on the first 250 months of the data and test on the next 100 months. For the OILMM, we use a range of numbers of latent processes, up to $m = p = 247$, and let the basis H be given by the eigenvectors of the kernel matrix over the points in space (Matérn–$5/2$ with a different length scale for latitude and longitude).

Tab. 1 summarises the performance of the models; more detailed graphs can be found in App. S. The OILMM achieves parity in RMSE with IGP at $m = 200$ latent processes—the data is highly periodic and the predictions are accurate for both models. Moreover, the OILMM requires only $m = 5$ latent processes to achieve a better PPLP than IGP and continues to improve with increasing m, demonstrating the need for a large number of latent processes.

4.4. Exchange Rates Prediction

In this experiment and the next, we test the orthogonality assumption and missing data approximation of the OILMM by comparing its performance to an equivalent ILMM with no restrictions on H and which deals exactly with missing data. We consider daily exchange rates with respect to USD of the top ten international currencies and three precious materials in the year 2007. The task is to predict CAD, JPY, and AUD on particular days given that all other currencies are observed throughout the whole year; we exactly follow Requeima et al. (2019) in the data and setup of the experiment. For the (O)ILMM, we use $m = 3$ latent processes with Matérn–$1/2$ kernels and randomly initialise and learn the basis H.

---

[3]3.6 GHz Intel Core i7 processor and 48 GB RAM

[4]All output from CMIP5 and ERA-Interim models was regridded onto the latitude–longitude grid used for the IPSL-CM5A-LR model.
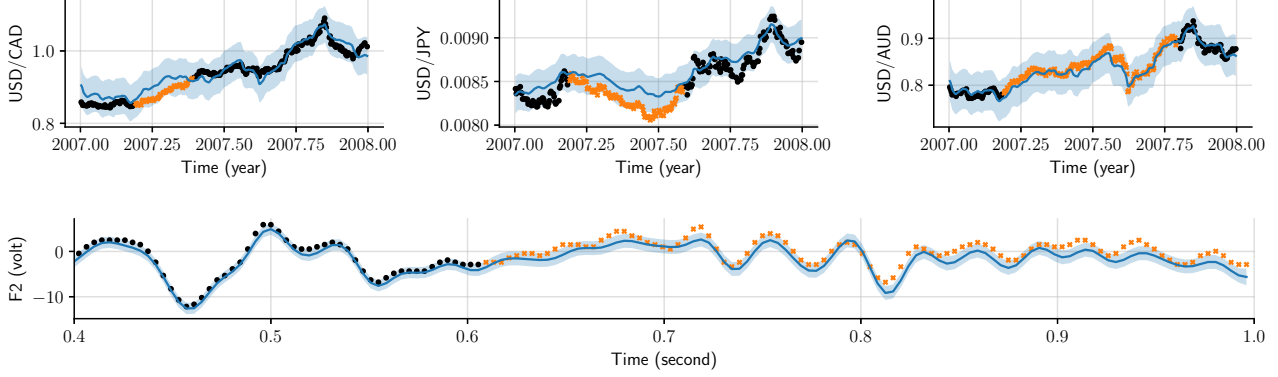
Figure 5. Predictions of the OILMM for the exchange rates experiment (top) and for one of the seven electrodes (F2) in the EEG experiment (bottom). Predictions are shown in blue, denoting the mean and central 95% credible region. Training data are denoted as black dots (●) and held-out test data as orange crosses (×).

Table 2. Standardised mean-squared error (SMSE) and normalised posterior predictive log-probability (PPLP) of held-out test data for various models in the exchange rates (ER) and EEG experiment. IGP stands for independent GPs. The references in square brackets are to models in Fig. 8 in App. B. GPAR (right column) is not a linear MOGP, and thus not comparable to the other methods. However, it is state-of-the-art on both tasks and hence provided as reference. The ILMM and OILMM achieve results equal up to two decimal places. *Numbers are taken from Nguyen & Bonilla (2014). †Numbers are taken from Requeima et al. (2019).

		IGP	CMOGP[11]	CGP[14]	ILMM	OILMM	GPAR[18]
SMSE	ER	0.60^*	0.24^*	0.21^*	0.19	0.19	$0.03^\dagger$
	EEG	$1.75^\dagger$			0.49	0.49	$0.26^\dagger$
PPLP	ER	3.57			3.39	3.39	
	EEG	-1.27			-2.11	-2.11	

Tab. 2 shows that the ILMM and OILMM have identical performance. This shows that the orthogonality assumption and missing data approximation of the OILMM can work well in practice.

4.5. Electroencephalogram Prediction

We consider 256 voltage measurements from 7 electrodes placed on a subject's scalp while the subject is shown a certain image; Zhang et al. (1995) describes the data collection process in detail. The task is to predict the last 100 samples for three electrodes given that the remainder of the data is observed; we exactly follow Requeima et al. (2019) in the data and setup of the experiment. For the (O)ILMM, we use $m = 3$ latent processes with exponentiated quadratic kernels and randomly initialise and learn H.

Tab. 2 shows that the ILMM and OILMM again have identical performance. This again shows that the orthogonality assumption does not harm the model's predictive power and that the missing data approximation can work well.

4.6. Large-Scale Climate model Calibration

In this final experiment, we scale to large data in a climate modelling task over Europe. We use the OILMM to find relationships between 28 climate simulators[4] (see Taylor et al., 2012, for background) by letting $H = H_s \otimes H_r$ (see App. H), where H_s are the first $m_s = 5$ eigenvectors of a 28×28 covariance matrix K_s between the simulators, and H_r are the first $m_r = 10$ eigenvectors of the kernel matrix over the points in space (Matérn–5/2 with a different length scale for latitude and longitude). This means that the $m_r m_s = 50$ latent processes are indexed by two indices i_s and i_r, one corresponding to the eigenvector of the simulator covariance and one to the eigenvector of the spatial covariance. The kernels for the latent processes are Matérn–5/2. We consider $n = 10000$ time points for all 28 simulators, each with 247 outputs, giving a total of roughly 70 million data points. For the independent problems, we use the variational inducing point method by Titsias (2009).

Fig. 6a shows that, as opposed to the empirical correlations, which ignore all temporal structure, the correlations learned by the OILMM exhibit a rich structure. A clustering of these correlations in Fig. 6b reveals that the identified structure is meaningful, because structurally similar simulators are grouped near each other. We conclude that the OILMM can be used to analyse large data in a simple and straightforward way, and is able to produce interpretable and meaningful results. See App. T for further experimental details and analysis of the results.

5. Discussion and Conclusion

We investigated the use of a sufficient statistic of the data to accelerate inference in MOGPs with orthogonal bases. In practice, the proposed methodology scales linearly with the number of latent processes m, allowing to scale to large m without sacrificing significant expressivity nor requiring any approximations. This is achieved by breaking down

(a) Empirical (left) and learned (right) correlations   (b) Clustering   (c) Latent processes
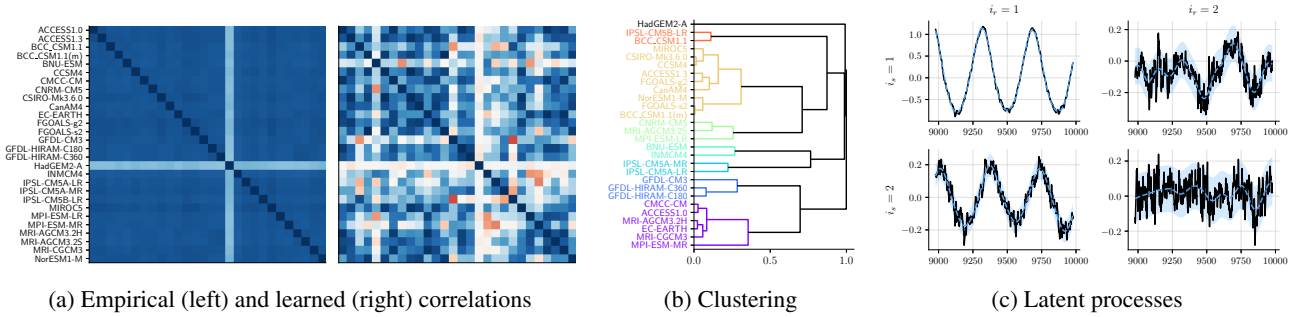
Figure 6. Results of the large-scale climate simulator experiment, showing (a) the empirical correlations and learned correlations (K_s) between the simulators, (b) a dendrogram deriving from hierarhically clustering the simulators based on the learned correlations where the colours indicate discovered groups, and (c) predictions for the latent processes for the first two eigenvectors of the covariance matrix between simulators $i_s = 1, 2$ and the first two eigenvectors of the spatial covariance $i_r = 1, 2$, for the last 1000 days. Predictions are shown in blue, denoting the mean and central 95% credible region.

the high-dimensional prediction problem into independent single-output problems, whilst retaining exact inference. As a consequence, the method is interpretable, extremely simple to implement, and trivially compatible with off-the-shelf single-output GP scaling techniques for handling large numbers of observations. We tested the method in a variety of experiments, demonstrating that it offers significant computational benefits without harming predictive performance. Interesting future directions are the application to non-Gaussian models for the latent processes (see Prop. 1) and targeting sub-linear time complexity by parallelisation (see, *e.g.*, Särkkä & García-Fernández, 2019).

Acknowledgements

References

Álvarez, M. and Lawrence, N. D. Sparse convolved Gaussian processes for multi-output regression. volume 21, pp. 57–64. Curran Associates, Inc., 2009.

Álvarez, M., Luengo, D., and Lawrence, N. Latent force models. 5:9–16, 2009.

Álvarez, M., Luengo, D., Titsias, M., and Lawrence, N. D. Efficient multioutput Gaussian processes through variational inducing kernels. In *Proceedings of the Thirteenth International Conference on Artificial Intelligence and Statistics*, volume 9 of *Proceedings of Machine Learning Research*, pp. 25–32. PMLR, 2010.

Álvarez, M. A. and Lawrence, N. D. Computationally efficient convolved multiple output Gaussian processes. *Journal of Machine Learning Research*, 12:1459–1500, 7 2011.

Bellouin, N., Collins, W., Culverwell, I., Halloran, P., Hardiman, S., Hinton, T., Jones, C., McDonald, R., McLaren, A., O'Connor, F., et al. The hadgem2 family of met office unified model climate configurations. *Geoscientific Model Development*, 4(3):723–757, 2011.

Bezanson, J., Edelman, A., Karpinski, S., and Shah, V. B. Julia: A fresh approach to numerical computing. *SIAM review*, 59(1):65–98, 2017.

Bi, D., Dix, M., Marsland, S. J., O'Farrell, S., Rashid, H., Uotila, P., Hirst, A., Kowalczyk, E., Golebiewski, M., Sullivan, A., et al. The access coupled model: description, control climate and evaluation. *Aust. Meteorol. Oceanogr. J*, 63(1):41–64, 2013.

Bonilla, E. V., Agakov, F. V., and Williams, C. K. I. Kernel multi-task learning using task-specific features. In *Proceedings of the Eleventh International Conference on Artificial Intelligence and Statistics*, volume 2 of *Proceedings of Machine Learning Research*, pp. 43–50. PMLR, 2007.

Bonilla, E. V., Chai, K. M., and Williams, C. K. I. Multi-task Gaussian process prediction. In *Advances in Neural Information Processing Systems*, volume 20, pp. 153–160. MIT Press, 2008.

Boyle, P. and Frean, M. Dependent Gaussian processes. In Saul, L. K., Weiss, Y., and Bottou, L. (eds.), *Advances in Neural Information Processing Systems 17*, pp. 217–224. MIT Press, 2005.

Brochu, E., Cora, V. M., and de Freitas, N. A tutorial on Bayesian optimization of expensive cost functions,

with application to active user modeling and hierarchical reinforcement learning. *arXiv preprint arXiv:1012.2599*, 12 2010.

Bruinsma, W. P. The generalised Gaussian convolution process model. Master's thesis, Department of Engineering, University of Cambridge, 2016.

Bui, T., Hernández-Lobato, D., Hernandez-Lobato, J., Li, Y., and Turner, R. Deep Gaussian processes for regression using approximate expectation propagation. pp. 1472–1481, 2016.

Bui, T. D., Yan, J., and Turner, R. E. A unifying framework for Gaussian process pseudo-point approximations using power expectation propagation. *Journal of Machine Learning Research*, 18(104):1–72, 2017.

Candela, J. Q. and Rasmussen, C. E. A unifying view of sparse approximate Gaussian process regression. *Journal of Machine Learning Research*, 6:1939–1959, 12 2005.

Casella, G. and Berger, R. *Statistical Inference*. Duxbury Resource Center, 6 2001.

Chen, J. and Revels, J. Robust benchmarking in noisy environments. *arXiv e-prints*, art. arXiv:1608.04295, Aug 2016.

Cheng, C.-A. and Boots, B. Variational inference for Gaussian process models with linear complexity. In *Advances in Neural Information Processing Systems*, pp. 5184–5194. Curran Associates, Inc., 2017.

Condit, R. *Tropical Forest Census Plots*. Springer-Verlag and R. G. Landes Company, Berlin, Germany, and Georgetown, Texas, 1998.

Dahl, A. and Bonilla, E. V. Grouped Gaussian processes for solar power prediction. *Machine Learning*, 108(8-9):1287–1306, 2019.

Damianou, A. *Deep Gaussian Processes and Variational Propagation of Uncertainty*. PhD thesis, Department of Neuroscience, University of Sheffield, 2015.

Dee, D. P., Uppala, S., Simmons, A., Berrisford, P., Poli, P., Kobayashi, S., Andrae, U., Balmaseda, M., Balsamo, G., Bauer, d. P., et al. The era-interim reanalysis: Configuration and performance of the data assimilation system. *Quarterly Journal of the royal meteorological society*, 137(656):553–597, 2011.

Deisenroth, M. P. and Rasmussen, C. E. PILCO: A model-based and data-efficient approach to policy search. volume 28, pp. 465–472. Omnipress, 2011.

Dezfouli, A., Bonilla, E. V., and Nock, R. Semi-parametric network structure discovery models. *arXiv preprint arXiv:1702.08530*, 2 2017.

Duvenaud, D. *Automatic Model Construction With Gaussian Processes*. PhD thesis, Computational and Biological Learning Laboratory, University of Cambridge, 2014.

Goovaerts, P. *Geostatistics for Natural Resources Evaluation*. Oxford University Press, 1 edition, 1997.

Hartikainen, J. and Särkkä, S. Kalman filtering and smoothing solutions to temporal Gaussian process regression models. In *Proceedings of the IEEE International Workshop on Machine Learning for Signal Processing (MLSP)*, pp. 379–384, 2010.

Hartikainen, J., Riihimäki, J., and Särkkä, S. Sparse spatio-temporal gaussian processes with general likelihoods. In *International Conference on Artificial Neural Networks*, pp. 193–200. Springer, 2011.

Hastings, W. K. Monte carlo sampling methods using markov chains and their applications. 1970.

Hennig, P., Osborne, M. A., and Girolami, M. Probabilistic numerics and uncertainty in computations. *Proceedings of the Royal Society of London A: Mathematical, Physical and Engineering Sciences*, 471(2179), 2015.

Hensman, J., Fusi, N., and Lawrence, N. D. Gaussian processes for big data. In *Proceedings of the 29th Conference on Uncertainty in Artificial Intelligence*, pp. 282–290, 2013.

Hensman, J., Durrande, N., and Solin, A. Variational fourier features for Gaussian processes. *Journal of Machine Learning Research*, 18(151):1–52, 2018.

Higdon, D., Gattiker, J., Williams, B., and Rightley, M. Computer model calibration using high-dimensional output. *Journal of the American Statistical Association*, 103 (482):570–583, 2008. ISSN 01621459. URL http://www.jstor.org/stable/27640080.

Hubbell, S., Foster, R., O'Brien, S., Harms, K., Condit, R., Wechsler, B., Wright, S., and De Lao, S. Light-gap disturbances, recruitment limitation, and tree diversity in a neotropical forest. *Science*, 283(5401):554–557, 1999.

Hubbell, S., Condit, R., and Foster, R. Barro colorado forest census plot data. URL https://ctfs.arnarb.harvard.edu/webatlas/datasets/bci, 2005.

Kaiser, M., Otte, C., Runkler, T., and Ek, C. H. Bayesian alignments of warped multi-output Gaussian processes. In *Advances in Neural Information Processing Systems*, pp. 6995–7004, 2018.

Kingma, D. P. and Welling, M. Auto-encoding variational Bayes. *arXiv preprint arXiv:1312.6114*, 12 2013.

Lázaro-Gredilla, M., Candela, J. Q., Rasmussen, C. E., and Figueiras-Vidal, A. R. Sparse spectrum Gaussian process regression. *Journal of Machine Learning Research*, 11: 1865–1881, 2010.

MacKay, D. J. C. *Information Theory, Inference & Learning Algorithms*. Cambridge University Press, 2002.

Matheron, G. Le krigeage universel. In *Cahiers du Centre de morphologie mathématique de Fontainebleau*, volume 1. École nationale supérieure des mines de Paris, 1969.

Minka, T. Deriving quadrature rules from Gaussian processes. Technical report, 2000.

MISO. Historical annual real-time LMPs, 2019. URL https://www.misoenergy.org/markets-and-operations/real-time--market-data/market-reports/#nt=%2FMarketReportType%3AHistorical%20LMP%2FMarketReportName%3AHistorical%20Annual%20Real-Time%20LMPs%20(zip)&t=10&p=0&s=MarketReportPublished&sd=desc.

Møller, J., Syversveen, A. R., and Waagepetersen, R. P. Log Gaussian Cox processes. *Scandinavian Journal of Statistics*, 25(3):451–482, 1998.

Murray, I. and Adams, R. P. Slice sampling covariance hyperparameters of latent Gaussian models. In *Advances in Neural Information Processing Systems*, volume 23, pp. 1732–1740. Curran Associates, Inc., 2010.

Murray, I., Adams, R., and MacKay, D. Elliptical slice sampling. In *Proceedings of the Thirteenth International Conference on Artificial Intelligence and Statistics*, volume 9 of *Proceedings of Machine Learning Research*, pp. 541–548. PMLR, 13–15 May 2010.

Nguyen, T. V. and Bonilla, E. V. Collaborative multi-output Gaussian processes. In *Conference on Uncertainty in Artificial Intelligence*, volume 30, 2014.

Nickisch, H., Solin, A., and Grigorievskiy, A. State space gaussian processes with non-gaussian likelihood. *arXiv preprint arXiv:1802.04846*, 2018.

Nocedal, J. and Wright, S. J. *Numerical Optimization*. Springer, 2 edition, 2006.

Osborne, M. A., Roberts, S. J., Rogers, A., Ramchurn, S. D., and Jennings, N. R. Towards real-time information processing of sensor network data using computationally

efficient multi-output Gaussian processes. In *Proceedings of the 7th International Conference on Information Processing in Sensor Networks*, IPSN '08, pp. 109–120. IEEE Computer Society, 2008.

Parra, G. and Tobar, F. Spectral mixture kernels for multi-output Gaussian processes. In *Advances in Neural Information Processing Systems*, pp. 6681–6690. Curran Associates, Inc., 2017.

Rasmussen, C. E. and Williams, C. K. I. *Gaussian Processes for Machine Learning*. MIT Press, 2006.

Requeima, J., Tebbutt, W., Bruinsma, W., and Turner, R. E. The Gaussian process autoregressive regression model (GPAR). In Chaudhuri, K. and Sugiyama, M. (eds.), *Proceedings of Machine Learning Research*, volume 89 of *Proceedings of Machine Learning Research*, pp. 1860–1869. PMLR, 4 2019.

Roweis, S. and Ghahramani, Z. A unifying review of linear Gaussian models. *Neural Computation*, 11(2):305–345, 1999. doi: 10.1162/089976699300016674. URL https://doi.org/10.1162/089976699300016674.

Saatçi, Y. *Scalable Inference for Structured Gaussian Process Models*. PhD thesis, University of Cambridge, Cambridge, UK, 2012.

Särkkä, S. and García-Fernández, Á. F. Temporal parallelization of Bayesian filters and smoothers. *arXiv preprint arXiv:1905.13002*, 5 2019.

Särkkä, S. and Solin, A. *Applied Stochastic Differential Equations*. Institute of Mathematical Statistics Textbooks. Cambridge University Press, 2019.

Särkkä, S., Solin, A., and Hartikainen, J. Spatiotemporal learning via infinite-dimensional Bayesian filtering and smoothing. *IEEE Signal Processing Magazine*, 30(4): 51–61, 2013.

Solin, A., Hensman, J., and Turner, R. E. Infinite-horizon Gaussian processes. In *Advances in Neural Information Processing Systems*, volume 31. Curran Associates, Inc., 2018.

Taylor, K. E., Stouffer, R. J., and Meehl, G. A. An overview of CMIP5 and the experiment design. *Bulletin of the American Meteorological Society*, 93(4):485–498, 2012.

Teh, Y. W. and Seeger, M. Semiparametric latent factor models. In *International Workshop on Artificial Intelligence and Statistics*, volume 10, 2005.

Tipping, M. E. and Bishop, C. M. Probabilistic principal component analysis. *Journal of the Royal Statistical Society, Series B*, 61(3):611–622, 1999.

Titsias, M. Variational learning of inducing variables in sparse Gaussian processes. In *Proceedings of the Twelth International Conference on Artificial Intelligence and Statistics*, volume 5 of *Proceedings of Machine Learning Research*, pp. 567–574. PMLR, 2009.

Tokdar, S. T. and Ghosh, J. K. Posterior consistency of logistic Gaussian process priors in density estimation. *Journal of Statistical Planning and Inference*, 137(1): 34–42, 2007.

Ulrich, K., Carlson, D. E., Dzirasa, K., and Carin, L. GP kernels for cross-spectrum analysis, 2015.

Wackernagel, H. *Multivariate Geostatistics*. Springer-Verlag Berlin Heidelberg, 3 edition, 2003.

Wilson, A. and Nickisch, H. Kernel interpolation for scalable structured Gaussian processes (KISS-GP). 37:1775–1784, 2015.

Wilson, A. G., Knowles, D. A., and Ghahramani, Z. Gaussian process regression networks. In *International Conference on Machine Learning*, volume 29. Omnipress, 2012.

Wu, T., Song, L., Li, W., Wang, Z., Zhang, H., Xin, X., Zhang, Y., Zhang, L., Li, J., Wu, F., et al. An overview of bcc climate system model development and application for climate change studies. *Journal of Meteorological Research*, 28(1):34–56, 2014.

Yu, B. M., Cunningham, J. P., Santhanam, G., Ryu, S. I., Shenoy, K. V., and Sahani, M. Gaussian-Process factor analysis for low-dimensional single-trial analysis of neural population activity. In *Advances in Neural Information Processing Systems*, volume 21, pp. 1881–1888. Curran Associates, Inc., 2009.

Zhang, X., Begleiter, H., Porjesz, B., Wang, W., and Litke, A. Event related potentials during object recognition tasks. *Brain Research Bulletin*, 38(6):531–538, 1995.

Zhe, S., Xing, W., and Kirby, R. M. Scalable high-order Gaussian process regression. In Chaudhuri, K. and Sugiyama, M. (eds.), *Proceedings of Machine Learning Research*, volume 89 of *Proceedings of Machine Learning Research*, pp. 2611–2620. PMLR, 4 2019.